

UC Berkeley

UC Berkeley Previously Published Works

Title

Defect passivation of transition metal dichalcogenides via a charge transfer van der Waals interface.

Permalink

<https://escholarship.org/uc/item/85x4f6vp>

Journal

Science advances, 3(10)

ISSN

2375-2548

Authors

Park, Jun Hong
Sanne, Atresh
Guo, Yuzheng
et al.

Publication Date

2017-10-01

DOI

10.1126/sciadv.1701661

Peer reviewed

SURFACE CHEMISTRY

Defect passivation of transition metal dichalcogenides via a charge transfer van der Waals interface

Jun Hong Park,^{1,2,3} Atresh Sanne,⁴ Yuzheng Guo,⁵ Matin Amani,⁶ Kehao Zhang,⁷ Hema C. P. Movva,⁴ Joshua A. Robinson,⁷ Ali Javey,⁶ John Robertson,⁸ Sanjay K. Banerjee,⁴ Andrew C. Kummel^{3,9*}

Integration of transition metal dichalcogenides (TMDs) into next-generation semiconductor platforms has been limited due to a lack of effective passivation techniques for defects in TMDs. The formation of an organic-inorganic van der Waals interface between a monolayer (ML) of titanyl phthalocyanine (TiOPc) and a ML of MoS₂ is investigated as a defect passivation method. A strong negative charge transfer from MoS₂ to TiOPc molecules is observed in scanning tunneling microscopy. As a result of the formation of a van der Waals interface, the $I_{\text{ON}}/I_{\text{OFF}}$ in back-gated MoS₂ transistors increases by more than two orders of magnitude, whereas the degradation in the photoluminescence signal is suppressed. Density functional theory modeling reveals a van der Waals interaction that allows sufficient charge transfer to remove defect states in MoS₂. The present organic-TMD interface is a model system to control the surface/interface states in TMDs by using charge transfer to a van der Waals bonded complex.

INTRODUCTION

Because silicon complementary metal-oxide semiconductor (CMOS) technology has scaled down to a few nanometers, the performance of CMOS transistors has faced fundamental limitations, such as short-channel effects (1, 2). Layered transition metal dichalcogenides (TMDs) have been considered as next-generation semiconductor platforms (3–5) because their atomically thin body allows enhanced electrostatic gate control and atomically scaled precision thickness control of the channel (6, 7) while suppressing the formation of undesired dangling bonds on the channel (8, 9). In addition, several TMDs exhibit a direct band gap in a monolayer (ML), thereby broadening their applications to potential candidates for optoelectronic devices (10, 11).

One major obstacle to using TMDs for semiconductor or optoelectronic platforms is the existence of intrinsic defects (12–16). Because of volatile chalcogens in the compounds, TMDs typically have a deficiency of chalcogen atoms at their surfaces, resulting in trapping states or undesirable doping (12). Moreover, surface adsorbates introduced from fabrication processing or ambient air can perturb the electronic or optical properties of TMDs (17). The existence of these surface defects mostly results in the degradation of the $I_{\text{ON}}/I_{\text{OFF}}$ ratio in field-effect transistors (FETs) or poor luminescence quantum yields (13–15). Therefore, effective surface passivation of TMDs is pivotal to obtaining high-performance devices.

To passivate defect states in TMDs, the passivation method should deactivate only the defect states without a permanent change in the intrinsic crystal and electronic structure of TMDs. Moreover, the adsorbed molecules should be chemically and thermally stable on TMDs; consequently, they should not decompose or desorb during the fabrication processes nor during operation under ambient conditions.

Surface treatments using substitution of extrinsic atoms or adsorption of molecules have been used to enhance photoluminescence (PL) (18–21), whereas the deposition of thick organic films to form p-n junctions has been used for potential photodetector applications (22). However, most of these treatments only improve the PL performance without enhancements of electronic performance, and the deposition of thick organic layers degrades electrical performance (20, 22).

Here, the deactivation of charged defect states is induced by the formation of an organic-inorganic van der Waals interface between single-layer titanyl phthalocyanine (TiOPc) and single-layer MoS₂. Metal phthalocyanines (MPcs) are known to form uniform structured interfaces with various metal and semiconductor surfaces because the planar structure of π -conjugated rings induces a flat-lying MPc/substrate configuration (23–25). Moreover, most MPcs have high thermal stability (26), and the flat-lying MPc/substrate structure ensures that the first layer of MPcs is more tightly bound than all other layers, enabling a simple postdeposition anneal to form a uniform ML of MPcs on TMDs. For passivation of TMDs, a single ML is used to simplify the bonding model. Among the various MPc molecules, TiOPc is chosen in this report to form a defect passivation layer, because it has an intrinsic net dipole at the central O-Ti group (27); consequently, a strong non-bonding interaction can be expected with MoS₂, without the direct disruption of phase and band structures in MoS₂. Strong charge transfer from MoS₂ to TiOPc is observed with scanning tunneling microscopy (STM) and spectroscopy (STS). Density functional theory (DFT) modeling is consistent with a van der Waals interaction that allows sufficient charge transfer to remove midgap states in MoS₂. As a result of the electric defect passivation at the TiOPc/MoS₂ interface, the $I_{\text{ON}}/I_{\text{OFF}}$ in the back-gated transistors is increased by more than two orders of magnitude with the improvements of a subthreshold slope (SS), whereas the degradation of PL is fully suppressed.

RESULTS

Sulfur vacancies can be observed on the planes of chemical vapor deposition (CVD) MoS₂ ML grown on highly oriented pyrolytic graphite (HOPG) (12, 28, 29). The present STM experiments were performed in an ultrahigh vacuum (UHV) (2×10^{-11} torr) at 100 K. As shown in Fig. 1A, the topographic STM image displays pinholes in the terrace

Copyright © 2017
The Authors, some
rights reserved;
exclusive licensee
American Association
for the Advancement
of Science. No claim to
original U.S. Government
Works. Distributed
under a Creative
Commons Attribution
NonCommercial
License 4.0 (CC BY-NC).

¹Center for Quantum Nanoscience, Institute for Basic Science (IBS), Seoul 03760, Republic of Korea. ²Department of Physics, Ewha Womans University, Seoul 03760, Republic of Korea. ³Materials Science and Engineering Program, University of California, San Diego, La Jolla, CA 92093, USA. ⁴Department of Electrical and Computer Engineering, University of Texas at Austin, Austin, TX 78712, USA. ⁵College of Engineering, Swansea University, Swansea, UK. ⁶Electrical Engineering and Computer Sciences, University of California at Berkeley, Berkeley, CA 94720, USA. ⁷Department of Materials Science and Engineering, Pennsylvania State University, University Park, PA 16802, USA. ⁸Department of Engineering, University of Cambridge, Cambridge CB2 1TN, UK. ⁹Departments of Chemistry and Biochemistry, University of California, San Diego, La Jolla, CA 92093, USA.

*Corresponding author. Email: akummel@ucsd.edu

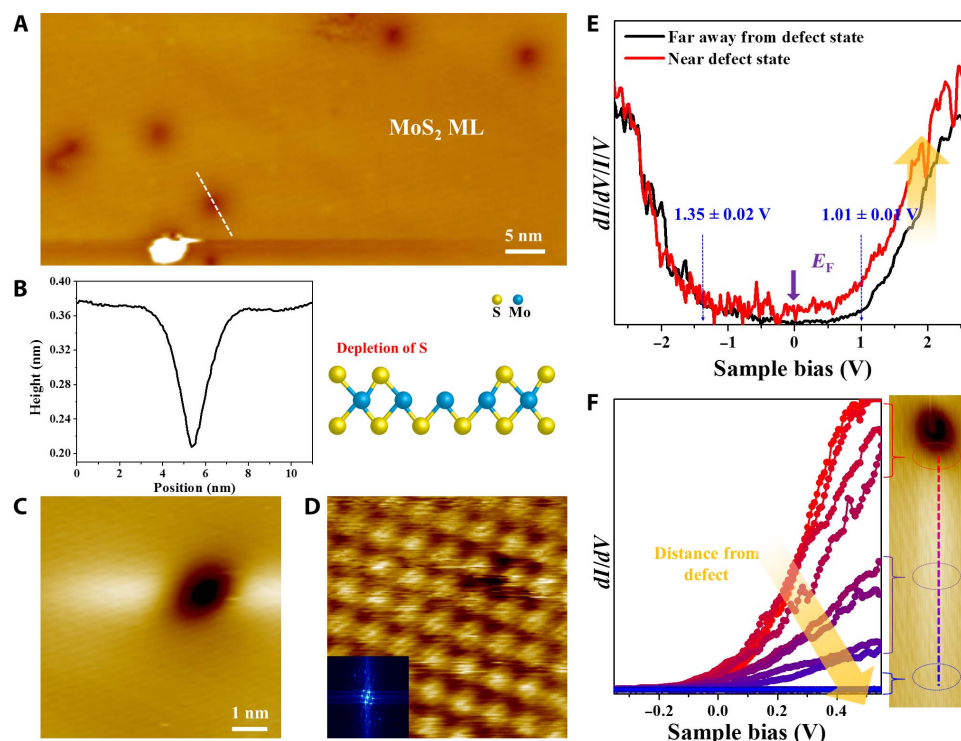


Fig. 1. Investigation of a bare ML MoS₂ surface deposited on HOPG. (A) Large-area STM image showing the ML MoS₂ terrace ($V_s = 2$ V, $I_t = 40$ pA). (B) Line trace analysis of the white line in (A) and the schematic model of defects in MoS₂. (C and D) Zoomed-in STM images of a single defect located on the ML MoS₂ in the empty ($V_s = 1$ V) and filled ($V_s = -1$ V) states, respectively ($I_t = 230$ pA). Scale bar, 1 nm; (D) at same magnification as (C). (E) STS measured on the terrace of a ML MoS₂; the black spectra are measured far away from the defects, whereas the red spectra are measured near a defect. (F) Spatial STS near the CB edge as a function of the distance from the defect.

of a ML MoS₂ flake; most of these defects are 1.5 Å deep and 2 nm in diameter, as shown in the left panel of Fig. 1B. On the basis of the present STM study and the previous published results (28, 29), these defects could be modeled as a few missing S atoms or both missing S and Mo atoms, as shown in the right panel of Fig. 1B. One of the defects is imaged via both empty-state (Fig. 1C) and filled-state modes (Fig. 1D) in an expanded STM image. Although the defects are shown as local depressions in both filled and empty states, the hexagonal atomic structure and the moiré pattern of the defects appear in only filled-state images.

A large electron population can be observed near defects of MoS₂, indicating that the vacancies in MoS₂ result in excess charge density (16), consistent with broken covalent bonds in the MoS₂ planes. As shown in the STS of Fig. 1E, two different local densities of states (LDOSs) are observed on MoS₂; a black STS, recorded far away from a defect in ML, has an apparent band gap of ~2.34 eV with a Fermi level (0 V) shifted to a conduction band (CB). This Fermi level is closer to the CB than to the valence band (VB) by about 0.3 V. Conversely, in the red STS, recorded close to a defect, large states are observed in the band gap, consistent with near metallic LDOS. The increase in band edge states results in an additional shift of the Fermi level toward the CB.

The band edge states are investigated by spatially resolved STS, as shown in Fig. 1F; multiple STSs were obtained adjacent to and far away from the defects. Large band edge states at the CB (shallow level) are observed when the tip is near a defect in MoS₂ (30). However, as the STM tip is moved away from the defects, the band edge states decrease significantly.

This negatively charged defect can be electrically deactivated by the adsorption of TiOPc molecules onto the MoS₂ ML. A few TiOPc molecules are deposited on MoS₂ MLs using molecular beam epitaxy at 300 K for 10 s, as shown in Fig. 2A. For sub-ML, the coverage of TiOPc molecules can be controlled by the deposition duration, as displayed in fig. S5. Each TiOPc molecule is observed as circular with a height of 0.3 nm, as shown in Fig. 2B, even though the TiOPc molecular structure is nearly square, as shown in the inset. It is hypothesized that single TiOPc molecules rotate on MoS₂ surfaces (31) because of the absence of locking, which is present at higher coverage.

To elucidate the electronic effects of single TiOPc molecule adsorption on MoS₂ MLs, spatially resolved STS is used, following a dashed arrow in Fig. 2C. In Fig. 2D, when the STM tip is positioned far away from the TiOPc molecules, the Fermi level is near the CB. However, as the STM tip approaches a TiOPc molecule, the Fermi level moves away from the CB to the middle of the band gap. Finally, positioning the STM tip near the TiOPc molecule results in the Fermi level moving close to the VB. From the present STS, it can be hypothesized that the excess negative charge in MoS₂ is transferred to TiOPc molecules. It is noted that although the deactivation of defect states via the adsorption of TiOPc molecules on MoS₂ relies on a charge transfer van der Waals interaction, as shown in fig. S7, other driving forces also might be used to passivate defect states, such as chemisorption on MoS₂. However, strong bonding forces can induce unintentional changes in the crystal or electric structure (32).

The TiOPc ML on the MoS₂ ML is investigated, as shown in Fig. 2E. With increasing deposition duration of TiOPc without postdeposition

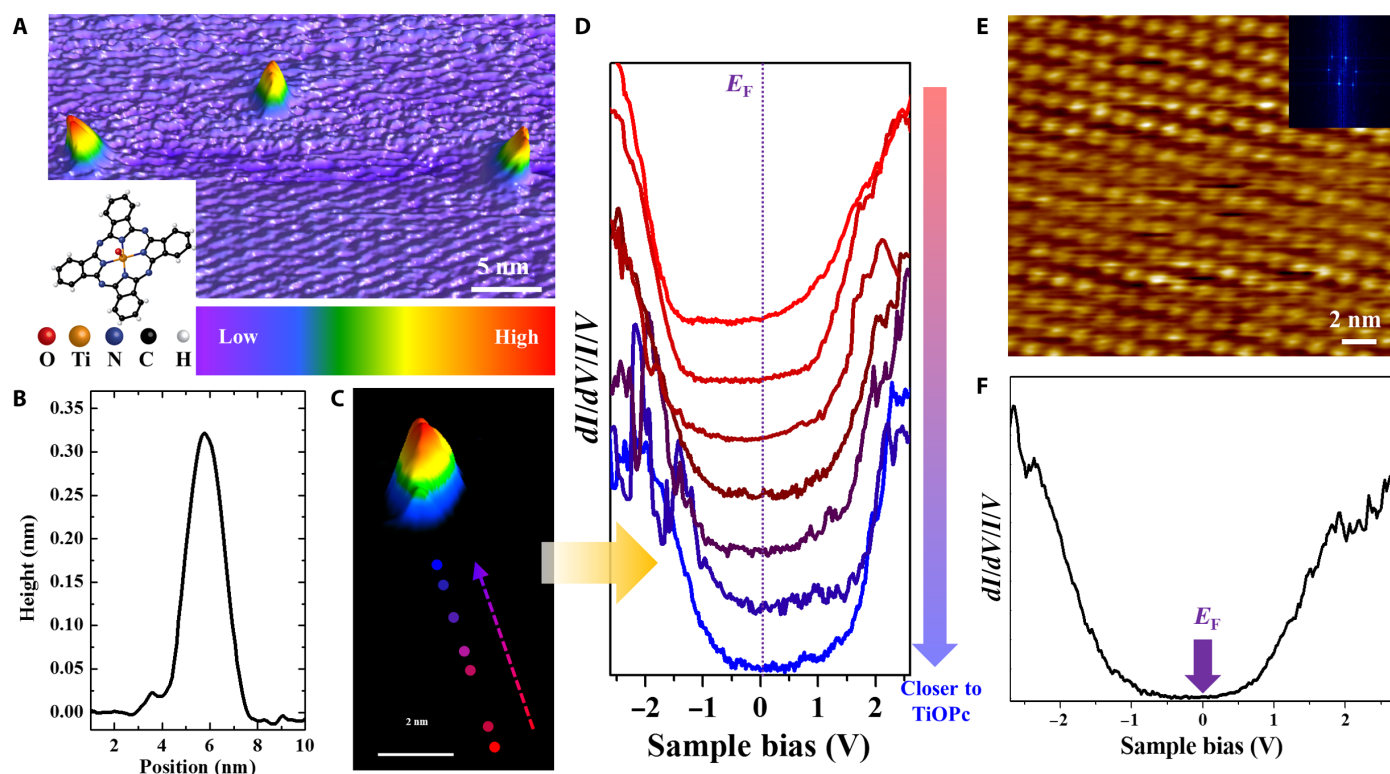


Fig. 2. Effects of the formation of the interface at TiOPc/MoS₂. (A) Few TiOPc molecules deposited on a MoS₂ ML at 300 K ($V_s = 2$ V, $I_t = 30$ pA). Inset shows the molecular structure of TiOPc. (B) Cross-sectional line trace of an adsorbed TiOPc molecule. (C) Single TiOPc adsorption with a black background. (D) Subset of dI/dV spectra taken along the dashed arrow in (C). (E) Formation of a full-coverage ML TiOPc on a ML MoS₂ and corresponding Fourier transform ($V_s = 2$ V, $I_t = 50$ pA). (F) STS of ML TiOPc on a ML MoS₂.

annealing, a hexagonal packed TiOPc ML is obtained with about 1.7-nm lateral spacing, and the center of each TiOPc molecule appears as a bright protrusion, consistent with the upward pointing of O–Ti to the vacuum (33). In the STS of Fig. 2E, a 1.7-eV band gap is observed with the Fermi level positioned near the lowest unoccupied molecular orbital. Once a TiOPc ML is formed on MoS₂, it is thermally stable on MoS₂, consistent with the tight binding between TiOPc and MoS₂, as shown in fig. S10. Note that because TiOPc molecules have only van der Waals interaction with the MoS₂ surface, it is hypothesized that the deposition of TiOPc does not induce the physical reconstructions of defects in the MoS₂.

DFT calculations are used to elucidate the change of the electronic structure in MoS₂ upon adsorption of TiOPc molecules. The projected density of states (PDOS) of a defect-free MoS₂ ML with two additional electrons is shown by a black curve in Fig. 3A; there are no observable states in the band gap. The two electrons were added to make the MoS₂ n-type consistent with the experimental data. S vacancies induce a large band gap state near the CB (orange dashed circle), as shown by the red curve, and reduce the band gap of 2e MoS₂. This defect state near the CB can also be observed in defective MoS₂ without the two electrons (neutral state), shown by an orange dashed circle in the blue curve. In both the 2e MoS₂ and the neutral MoS₂ cases, the defect states can be observed near the CB edges, consistent with the existence of defect states at shallow levels (30). These band gap states near the CB can result in unintentional doping or trapping states in transistors (12, 14–16). The DFT model of TiOPc passivation consisting of two TiOPc molecules on top of the MoS₂ with a single S vacancy is shown in Fig. 3B. As shown in Fig. 3C, the band edge states are suppressed, and the band gap is re-

stored to the original size in the PDOS of MoS₂, consistent with electric deactivation of defect states. It is noted that a tiny state is observed at -0.8 eV in PDOS of MoS₂. This state corresponds to the highest occupied molecular orbital of TiOPc (red curve) in TiOPc/MoS₂, and it is included in the PDOS of MoS₂ during the projections of orbitals.

To understand the source of passivation, the charge was calculated as shown in the Supplementary Materials. For the TiOPc passivated S(Vac)/MoS₂ system with a net -2 charge, each TiOPc adsorbs a charge of 0.8 electrons, as shown in table S2. Even for an uncharged TiOPc passivated MoS₂ system, each TiOPc adsorbs a charge of 0.5 electrons. This is consistent with previous studies showing aromatic molecules that lower the work function in metal surfaces via charge transfer (34).

The electrical characteristics of a four-point back-gated single-layer MoS₂ FET (channel length of 10 μ m and width of 3 μ m) with/without a TiOPc passivation layer are investigated at a drain bias of 1 V, as shown in Fig. 4A. The black transfer curve is the sweep of bare MoS₂ showing a threshold voltage, V_{TH} , of about -14 V with an I_{ON}/I_{OFF} ratio of 10^4 . This depletion mode V_{TH} is undesirably shifted to negative voltages, which is indicative of S vacancies in the channel and extrinsic charge dopants from the substrate (35). As shown in the red curve, the annealing of the same MoS₂ FET in a UHV further degrades the I_{ON}/I_{OFF} ratio with a negligible shift of the V_{TH} . Conversely, after the deposition of a TiOPc ML on the same MoS₂ FET, the I_{ON}/I_{OFF} improves to greater than 10^7 , because of a 100 \times reduction of the OFF-state leakage and a return of an ON-state drive current to the preannealed levels. In addition, the V_{TH} positively shifts to 10 V because the TiOPc compensates for the excess charge. The SS below

the V_{TH} also are improved from 6.7 to 1.6 V/dec by the deposition of a TiOPc ML, suggesting the deactivation of some of the channel defects.

The deposition of TiOPc ML does not induce degradation of the PL of a ML MoS₂ (Fig. 4B). To track the change in PL of MoS₂ upon TiOPc deposition, we performed measurements on the same flake after exfoliation, annealing of MoS₂ at 597 K in a UHV, and TiOPc deposition. Before annealing, the MoS₂ ML shows low luminescence with a broad spectrum, which can be attributed to emission from both free excitons and charged trions, which is typically observed in exfoliated MoS₂. After annealing, a 2× increase is observed in PL. Moreover, the overall full width at half maximum (FWHM) decreases from 95 to 52 meV, and the emission from the charged trion is quenched. An additional increase of PL intensity is observed after the deposition of a ML TiOPc on the annealed ML MoS₂ with no change in the FWHM. In addition, a 20-meV

red shift is observed in the emission compared to annealed MoS₂, consistent with a 10-meV blue shift from bare MoS₂ (36). This modest improvement in TiOPc/MoS₂ could be interpreted as an increase in the quantum yield of excitons by the transfer of excess charge to TiOPc (37).

DISCUSSION

The electrical deactivation of defect states at the interface of TiOPc/MoS₂ has been elucidated using STM and STS. The depletion of sulfur results in an intrinsic n-shifted electronic structure in bare MoS₂, whereas the formation of a TiOPc/MoS₂ interface induces a negative charge transfer from MoS₂ to TiOPc. It is noted that although there is no clear evidence that defect sites can provide preferable adsorption sites for TiOPc molecules during observation in STM, it can be hypothesized

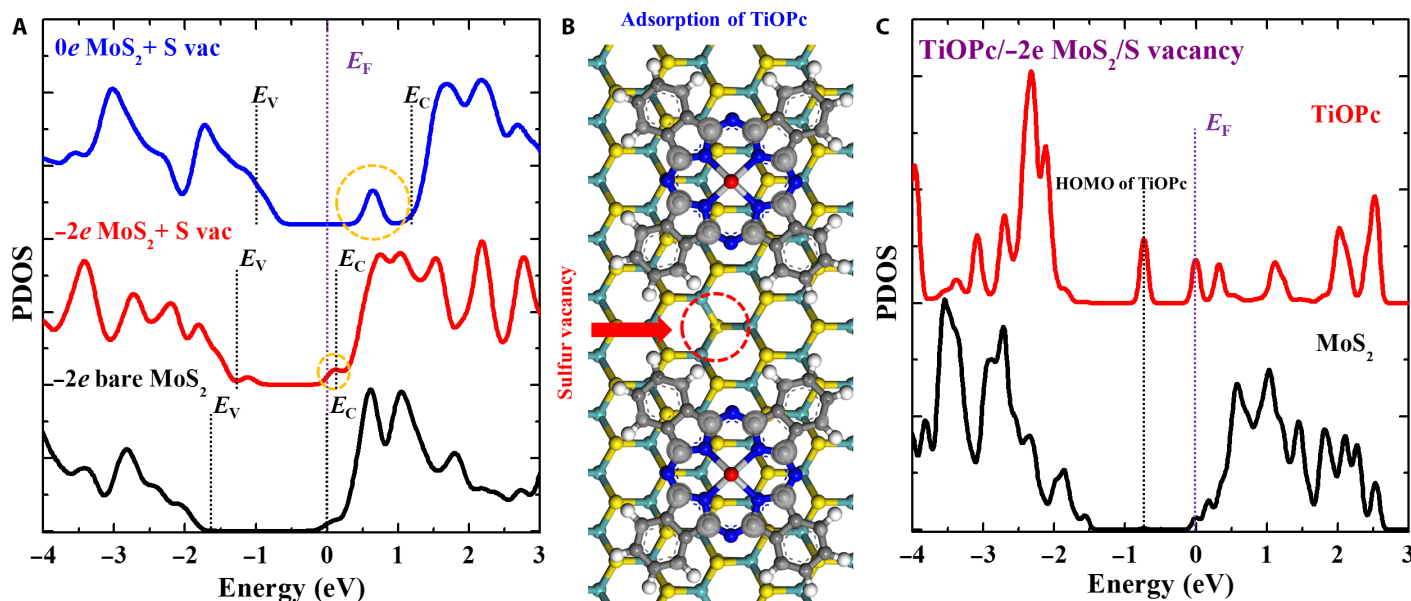


Fig. 3. DFT of TiOPc molecules adsorbed on ML MoS₂. (A) PDOS of MoS₂ with no defects and a sulfur vacancy. (B) Absorption of two TiOPc molecules on MoS₂ with a sulfur vacancy. (C) PDOS of TiOPc and MoS₂ in TiOPc/MoS₂. HOMO, highest occupied molecular orbital.

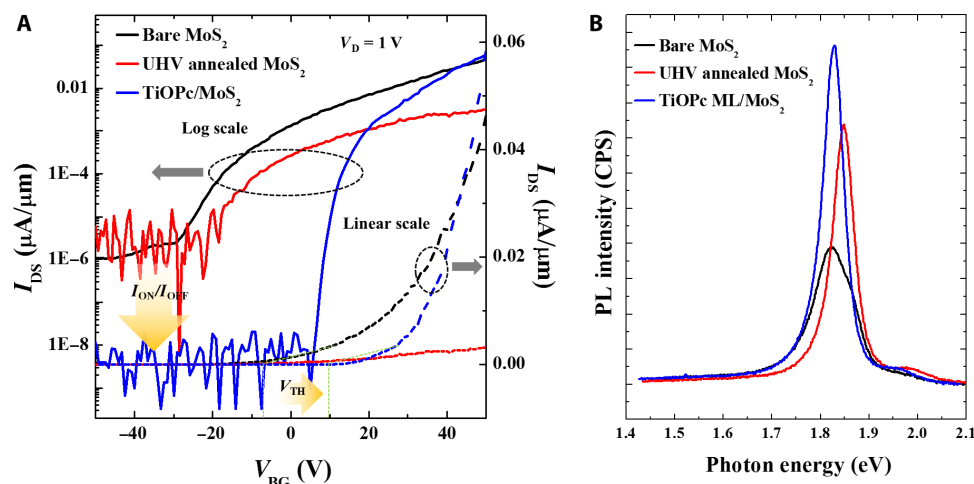


Fig. 4. Electrical and PL characteristics of MoS₂ ML, with and without ML TiOPc. (A) Back-gated transfer characteristics of a ML MoS₂ FET in log (solid curves) and linear (dashed curves) scales, before and after deposition of ML TiOPc. (B) Room temperature PL of exfoliated ML MoS₂ before and after deposition of ML TiOPc. CPS, counts per second.

that the total amount of charge transfer from a ML MoS_2 to adsorbed TiOPc molecules can be tuned by the coverage of TiOPc molecules on MoS_2 . Moreover, the van der Waals interaction at the interface of TiOPc and MoS_2 , such as the direction of charge transfer or the amount of charge transfer, might be tuned by chemical functionalization of the MPcs, such as adding additional groups to the benzene rings or modifications of central atoms. For example, bare CuPc molecules are p-type complexes under ambient conditions, whereas F_{16}CuPc molecules are n-type complexes under ambient conditions (38, 39); consequently, the charge transfer with TMDs might be modified by the ligands on the MPcs. DFT reveals that formation of a van der Waals interface induces suppression of defect states in MoS_2 . As a result, the $I_{\text{ON}}/I_{\text{OFF}}$ ratio and the SS in back-gated FET are greatly improved by the selective deactivation of defect states via the deposition of ML TiOPc, without changes in the band structure of MoS_2 nor degradation of the PL intensity, as shown in STM/STS, DFT, and PL. Conversely, the previous results for TMDs passivated chemically via an introduction of extrinsic atoms involved a permanent transition in crystal structure and therefore induced a change in the band gap of TMDs (40, 41). Adsorption of other organic molecules, such as alkanethiol or thick organic layers, also induced the degradations of the $I_{\text{ON}}/I_{\text{OFF}}$ ratio in MoS_2 FETs (20, 22). It is noted that in the present STM/STS and the DFT data, the defect states at shallow energy levels (near a CB edge) can be observed with S vacancies, whereas defects at deep energy levels (in the middle of a band gap) cannot be observed in STM/STS. Because the present TiOPc/ MoS_2 charge transfer van der Waals interface relies on the nonbonding interaction, it may have limitations in passivating deep-level defect states. For deep-level defects, a strong interaction, such as chemical reaction, may be required. Therefore, the present result suggests that the defect states in TMDs can be controlled and passivated via using van der Waals interface with organic ML.

MATERIALS AND METHODS

MoS_2 ML was prepared via two different methods, CVD growth and mechanical exfoliation from bulk. The details are included in the Supplementary Materials.

The TiOPc powder (95% purity) purchased from Sigma-Aldrich was purified by multiple sublimations with a differentially pumped effusion cell (Eberl MBE-Komponenten) attached to a UHV STM chamber. Afterward, the effusion cell was heated to 633 K with a rate of 1 K/s, while the MoS_2 /HOPG samples were placed in a UHV chamber. During the deposition of TiOPc, the sample temperature was held at 300 K, and the coverage of TiOPc on MoS_2 was controlled by the deposition duration, as shown in the below separated part.

STM and STS (Omicron VT STM) were performed in a UHV chamber (2×10^{-11} torr) using electrochemically etched tungsten tips, while the samples were cooled at 100 K using liquid nitrogen. Before performing STM and STS on MoS_2 /HOPG or TiOPc/ MoS_2 /HOPG, the STM tips were calibrated on an Si (100) surface and bare HOPG surfaces.

SUPPLEMENTARY MATERIALS

Supplementary material for this article is available at <http://advances.sciencemag.org/cgi/content/full/3/10/e1701661/DC1>

Supplementary Materials and Methods

fig. S1. The SEM of as-grown MoS_2 on HOPG via CVD showing two different areas.

fig. S2. STS of MoS_2 ML taken far away from defects with fitting in a linear scale.

fig. S3. The large-area STM image of bare MoS_2 grown by CVD on HOPG.

fig. S4. Raman spectra of a MoS_2 ML before and after deposition of TiOPc under a 488-nm laser excitation.

fig. S5. The deposition of TiOPc molecules on MoS_2 ML via molecular beam epitaxy at 300 K.

fig. S6. Reproduced subset of $dI/dV/I/V$ near the TiOPc molecule on MoS_2 ML.

fig. S7. Tip-induced diffusion of TiOPc molecule on MoS_2 .

fig. S8. STM image and STS recorded in bulk MoS_2 -deposited TiOPc molecules.

fig. S9. Full ML of TiOPc on bulk MoS_2 and corresponding STS of a TiOPc ML.

fig. S10. Thermal stability of a TiOPc ML on an MoS_2 ML.

fig. S11. DFT calculations of net charge in a TiOPc/ MoS_2 ML; three different locations in MoS_2 ML are selected, as shown in the circles.

fig. S12. Back-gated leakage current of a single-layer MoS_2 FET, with $V_D = 1$ V before and after deposition of a TiOPc ML.

fig. S13. Back-gated transfer characteristics of a single-layer MoS_2 FET, with $V_D = 0.1$ V before and after deposition of a TiOPc ML.

table S1. Summary of relative net charge of TiOPc and MoS_2 (neutral) from three different locations.

table S2. Net charge of TiOPc and MoS_2 ($-2e$).

References (33, 42–60)

REFERENCES AND NOTES

1. T. Sakurai, Perspectives of low-power VLSI's. *IEICE Trans. Electron.* **E87-C**, 429–436 (2004).
2. A. D. Franklin, Nanomaterials in transistors: From high-performance to thin-film applications. *Science* **349**, aab2750 (2015).
3. B. Radisavljevic, A. Radenovic, J. Brivio, V. Giacometti, A. Kis, Single-layer MoS_2 transistors. *Nat. Nanotechnol.* **6**, 147–150 (2011).
4. D. Jena, Tunneling transistors based on graphene and 2-D crystals. *Proc. IEEE* **101**, 1585–1602 (2013).
5. S. B. Desai, S. R. Madhupathy, A. B. Sachid, J. P. Llinas, Q. Wang, G. H. Ahn, G. Pitner, M. J. Kim, J. Bokor, C. Hu, H.-S. P. Wong, A. Javey, MoS_2 transistors with 1-nanometer gate lengths. *Science* **354**, 99–102 (2016).
6. E. Suzuki, K. Ishii, S. Kanamaru, T. Maeda, T. Tsutsumi, T. Sekigawa, K. Nagai, H. Hiroshima, Highly suppressed short-channel effects in ultrathin SOI n-MOSFETs. *IEEE Trans. Electron. Dev.* **47**, 354–359 (2000).
7. M. Luisier, M. Lundstrom, D. A. Antoniadis, J. Bokor, Ultimate device scaling: Intrinsic performance comparisons of carbon-based, InGaAs, and Si field-effect transistors for 5 nm gate length, 2011 IEEE International Electron Devices Meeting (IEDM 2011), Washington, DC, 5 to 7 December 2011.
8. H. Fang, C. Battaglia, C. Carraro, S. Nemsak, B. Ozdol, J. S. Kang, H. A. Bechtel, S. B. Desai, F. Kronast, A. A. Unal, G. Conti, C. Conlon, G. K. Palsson, M. C. Martin, A. M. Minor, C. S. Fadley, E. Yablonovitch, R. Maboudian, A. Javey, Strong interlayer coupling in van der Waals heterostructures built from single-layer chalcogenides. *Proc. Natl. Acad. Sci. U.S.A.* **111**, 6198–6202 (2014).
9. C.-H. Lee, G.-H. Lee, A. M. van der Zande, W. Chen, Y. Li, M. Han, X. Cui, G. Arefe, C. Nuckolls, T. F. Heinz, J. Guo, J. Hone, P. Kim, Atomically thin p-n junctions with van der Waals heterointerfaces. *Nat. Nanotechnol.* **9**, 676–681 (2014).
10. S. Wu, S. Buckley, J. R. Schaibley, L. Feng, J. Yan, D. G. Mandrus, F. Hatami, W. Yao, J. Vučković, A. Majumdar, X. Xu, Monolayer semiconductor nanocavity lasers with ultralow thresholds. *Nature* **520**, 69–72 (2015).
11. C. Palacios-Berraquero, M. Barbone, D. M. Kara, X. Chen, I. Goykhman, D. Yoon, A. K. Ott, J. Beitner, K. Watanabe, T. Taniguchi, A. C. Ferrari, M. Atatüre, Atomically thin quantum light-emitting diodes. *Nat. Commun.* **7**, 12978 (2016).
12. K. C. Santosh, R. C. Longo, R. Addou, R. M. Wallace, K. Cho, Impact of intrinsic atomic defects on the electronic structure of MoS_2 monolayers. *Nanotechnology* **25**, 375703 (2014).
13. H. N. Wang, C. J. Zhang, F. Rana, Ultrafast dynamics of defect-assisted electron-hole recombination in mono layer MoS_2 . *Nano Lett.* **15**, 339–345 (2015).
14. Z. Yu, Y. Pan, Y. Shen, Z. Wang, Z.-Y. Ong, T. Xu, R. Xin, L. Pan, B. Wang, L. Sun, J. Wang, G. Zhang, Y. W. Zhang, Y. Shi, X. Wang, Towards intrinsic charge transport in monolayer molybdenum disulfide by defect and interface engineering. *Nat. Commun.* **5**, 5290 (2014).
15. Z. Wu, Z. Luo, Y. Shen, W. Zhao, W. Wang, H. Nan, X. Guo, L. Sun, X. Wang, Y. You, Z. Ni, Defects as a factor limiting carrier mobility in WSe_2 : A spectroscopic investigation. *Nano Res.* **9**, 3622–3631 (2016).
16. D. Liu, Y. Guo, L. Fang, J. Robertson, Sulfur vacancies in monolayer MoS_2 and its electrical contacts. *Appl. Phys. Lett.* **103**, 183113 (2013).
17. S. H. Chae, Y. Jin, T. S. Kim, D. S. Chung, H. Na, H. Nam, H. Kim, D. J. Perello, H. Y. Jeong, T. H. Ly, Y. H. Lee, Oxidation effect in octahedral hafnium disulfide thin film. *ACS Nano* **10**, 1309–1316 (2016).
18. H. Nan, Z. Wang, W. Wang, Z. Liang, Y. Lu, Q. Chen, D. He, P. Tan, F. Miao, X. Wang, J. Wang, Z. Ni, Strong photoluminescence enhancement of MoS_2 through defect engineering and oxygen bonding. *ACS Nano* **8**, 5738–5745 (2014).

19. M. Amani, D.-H. Lien, D. Kiriya, J. Xiao, A. Azcatl, J. Noh, S. R. Madhupathy, R. Addou, K. C. Santos, M. Dubey, K. Cho, R. M. Wallace, S.-C. Lee, J.-H. He, J. W. Ager III, X. Zhang, E. Yablonovitch, A. Javey, Near-unity photoluminescence quantum yield in MoS₂. *Science* **350**, 1065–1068 (2015).
20. K. Cho, M. Min, T.-Y. Kim, H. Jeong, J. Pak, J.-K. Kim, J. Jang, S. J. Yun, Y. H. Lee, W.-K. Hong, T. Lee, Electrical and optical characterization of MoS₂ with sulfur vacancy passivation by treatment with alkanethiol molecules. *ACS Nano* **9**, 8044–8053 (2015).
21. H.-V. Han, A.-Y. Lu, L.-S. Lu, J.-K. Huang, H. Li, C.-L. Hsu, Y.-C. Lin, M. H. Chiu, K. Suenaga, C.-W. Chu, H.-C. Kuo, W.-H. Chang, L.-J. Li, Y. Shi, Photoluminescence enhancement and structure repairing of monolayer MoSe₂ by hydrohalic acid treatment. *ACS Nano* **10**, 1454–1461 (2016).
22. J. Pak, J. Jang, K. Cho, T.-Y. Kim, J.-K. Kim, Y. Song, W.-K. Hong, M. Min, H. Lee, T. Lee, Enhancement of photodetection characteristics of MoS₂ field effect transistors using surface treatment with copper phthalocyanine. *Nanoscale* **7**, 18780–18788 (2015).
23. K. Xiao, W. Deng, J. K. Keum, M. Yoon, I. V. Vlassiouk, K. W. Clark, A.-P. Li, I. I. Kravchenko, G. Gu, E. A. Payzant, B. G. Sumpter, S. C. Smith, J. F. Browning, D. B. Geohegan, Surface-induced orientation control of CuPc molecules for the epitaxial growth of highly ordered organic crystals on graphene. *J. Am. Chem. Soc.* **135**, 3680–3687 (2013).
24. Z. Li, B. Li, J. Yang, J. G. Hou, Single-molecule chemistry of metal phthalocyanine on noble metal surfaces. *Acc. Chem. Res.* **43**, 954–962 (2010).
25. P. Gargiani, M. Angelucci, C. Mariani, M. G. Betti, Metal-phthalocyanine chains on the Au(110) surface: Interaction states versus *d*-metal states occupancy. *Phys. Rev. B* **81**, 085412 (2010).
26. J. D. Wright, Gas-adsorption on phthalocyanines and its effects on electrical-properties. *Prog. Surf. Sci.* **31**, 1–60 (1989).
27. Y. Wei, S. W. Robey, J. E. Reutt-Robey, Flux-selected titanyl phthalocyanine monolayer architecture on Ag (111). *J. Phys. Chem. C* **112**, 18537–18542 (2008).
28. P. Vancsó, G. Z. Magda, J. Pető, J.-Y. Noh, Y.-S. Kim, C. Hwang, L. P. Biró, L. Tapasztó, The intrinsic defect structure of exfoliated MoS₂ single layers revealed by Scanning Tunneling Microscopy. *Sci. Rep.* **6**, 29726 (2016).
29. W. Zhou, X. Zou, S. Najmaei, Z. Liu, Y. Shi, J. Kong, J. Lou, P. M. Ajayan, B. I. Yakobson, J.-C. Idrobo, Intrinsic structural defects in monolayer molybdenum disulfide. *Nano Lett.* **13**, 2615–2622 (2013).
30. M. Pandey, F. A. Rasmussen, K. Kuhar, T. Olsen, K. W. Jacobsen, K. S. Thygesen, Defect-tolerant monolayer transition metal dichalcogenides. *Nano Lett.* **16**, 2234–2239 (2016).
31. H. L. Tierney, C. E. Calderon, A. E. Baber, E. C. H. Sykes, F. Wang, Understanding the rotational mechanism of a single molecule: STM and DFT investigations of dimethyl sulfide molecular rotors on Au(111). *J. Phys. Chem. C* **114**, 3152–3155 (2010).
32. M. Kang, B. Kim, S. H. Ryu, S. W. Jung, J. Kim, L. Moreschini, C. Jozwiak, E. Rotenberg, A. Bostwick, K. S. Kim, Universal mechanism of band-gap engineering in transition-metal dichalcogenides. *Nano Lett.* **17**, 1610–1615 (2017).
33. I. Kröger, B. Stadtmüller, C. Kumpf, Submonolayer and multilayer growth of titaniumoxide-phthalocyanine on Ag(111). *New J. Phys.* **18**, 113022–1–113022-20 (2016).
34. A. Bilić, J. R. Reimers, N. S. Hush, R. C. Hoft, M. J. Ford, Adsorption of benzene on copper, silver, and gold surfaces. *J. Chem. Theory Comput.* **2**, 1093–1105 (2006).
35. A. Sanne, R. Ghosh, A. Rai, M. N. Yogesh, S. H. Shin, A. Sharma, K. Jarvis, L. Mathew, R. Rao, D. Akinwande, S. Banerjee, Radio frequency transistors and circuits based on CVD MoS₂. *Nano Lett.* **15**, 5039–5045 (2015).
36. K. F. Mak, K. He, C. Lee, G. H. Lee, J. Hone, T. F. Heinz, J. Shan, Tightly bound trions in monolayer MoS₂. *Nat. Mater.* **12**, 207–211 (2013).
37. W. Su, H. Dou, D. Huo, N. Dai, L. Yang, Enhancing photoluminescence of trion in single-layer MoS₂ using *p*-type aromatic molecules. *Chem. Phys. Lett.* **635**, 40–44 (2015).
38. D. G. de Oteyza, E. Barrena, J. O. Ossó, H. Dosch, S. Meyer, J. Pflaum, Controlled enhancement of the electron field-effect mobility of F₁₆CuPc thin-film transistors by use of functionalized SiO₂ substrates. *Appl. Phys. Lett.* **87**, 183504 (2005).
39. Z. Bao, A. J. Lovinger, A. Dodabalapur, Organic field-effect transistors with high mobility based on copper phthalocyanine. *Appl. Phys. Lett.* **69**, 3066–3068 (1996).
40. H.-P. Komsa, A. V. Krasheninnikov, Two-dimensional transition metal dichalcogenide alloys: Stability and electronic properties. *J. Phys. Chem. Lett.* **3**, 3652–3656 (2012).
41. A. Kutana, E. S. Penev, B. I. Yakobson, Engineering electronic properties of layered transition-metal dichalcogenide compounds through alloying. *Nanoscale* **6**, 5820–5825 (2014).
42. S. McDonnell, R. Addou, C. Buie, R. M. Wallace, C. L. Hinkle, Defect-dominated doping and contact resistance in MoS₂. *ACS Nano* **8**, 2880–2888 (2014).
43. K. Zhang, S. Feng, J. Wang, A. Azcatl, N. Lu, R. Addou, N. Wang, C. Zhou, J. Lerach, V. Bojan, M. J. Kim, L.-Q. Chen, R. M. Wallace, M. Terrones, J. Zhu, J. A. Robinson, Correction to manganese doping of monolayer MoS₂: The substrate is critical. *Nano Lett.* **16**, 2125 (2016).
44. L. Chen, B. Liu, M. Ge, Y. Ma, A. N. Abbas, C. Zhou, Step-edge-guided nucleation and growth of aligned WSe₂ on sapphire via a layer-over-layer growth mode. *ACS Nano* **9**, 8368–8375 (2015).
45. L. Jiao, H. J. Liu, J. L. Chen, Y. Yi, W. G. Chen, Y. Cai, J. N. Wang, X. Q. Dai, N. Wang, W. K. Ho, M. H. Xie, Molecular-beam epitaxy of monolayer MoSe₂: Growth characteristics and domain boundary formation. *New J. Phys.* **17**, 053023 (2015).
46. R. M. Feenstra, Tunneling spectroscopy of the (110) surface of direct-gap III-V Semiconductors. *Phys. Rev. B* **50**, 4561–4570 (1994).
47. R. M. Feenstra, J. Y. Lee, M. H. Kang, G. Meyer, K. H. Rieder, Band gap of the Ge(111)c(2x8) surface by scanning tunneling spectroscopy. *Phys. Rev. B* **73**, 035310 (2006).
48. P. R. Bevington, D. K. Robinson, *Data Reduction and Error Analysis for the Physical Sciences* (McGraw-Hill, ed. 3, 2003).
49. M. D. Segall, P. J. D. Lindan, M. J. Probert, C. J. Pickard, P. J. Hasnip, S. J. Clark, M. C. Payne, First-principles simulation: Ideas, illustrations and the CASTEP code. *J. Phys. Condens. Matter* **14**, 2717–2744 (2002).
50. A. Tkatchenko, M. Scheffler, Accurate molecular van der Waals interactions from ground-state electron density and free-atom reference data. *Phys. Rev. Lett.* **102**, 073005 (2009).
51. Z. Yin, H. Li, H. Li, L. Jiang, Y. Shi, Y. Sun, G. Lu, Q. Zhang, X. Chen, H. Zhang, Single-layer MoS₂ phototransistors. *ACS Nano* **6**, 74–80 (2012).
52. Y. L. Huang, Y. Chen, W. Zhang, S. Y. Quek, C.-H. Chen, L.-J. Li, W.-T. Hsu, W.-H. Chang, Y. J. Zheng, W. Chen, A. T. S. Wee, Bandgap tunability at single-layer molybdenum disulfide grain boundaries. *Nat. Commun.* **6**, 6298 (2015).
53. A. Tuxen, J. Kibsgaard, G. Gobel, E. Lægsgaard, H. Topsøe, J. V. Lauritsen, F. Besenbacher, Size threshold in the dibenzothiophene adsorption on MoS₂ nanoclusters. *ACS Nano* **4**, 4677–4682 (2010).
54. C. Tsai, F. Abild-Pedersen, J. K. Nørskov, Tuning the MoS₂ edge-site activity for hydrogen evolution via support interactions. *Nano Lett.* **14**, 1381–1387 (2014).
55. A. Bruix, H. G. Fächtbauer, A. K. Tuxen, A. S. Walton, N. Andersen, S. Porsgaard, F. Besenbacher, B. Hammer, J. V. Lauritsen, In situ detection of active edge sites in single-layer MoS₂ catalysts. *ACS Nano* **9**, 9322–9330 (2015).
56. C. Lee, H. Yan, L. E. Brus, T. F. Heinz, J. Hone, S. Ryu, Anomalous lattice vibrations of single- and few-layer MoS₂. *ACS Nano* **4**, 2695–2700 (2010).
57. S. C. B. Mannsfeld, T. Fritz, Understanding organic–inorganic heteroepitaxial growth of molecules on crystalline substrates: Experiment and theory. *Phys. Rev. B* **71**, 235405 (2005).
58. X.-H. Kong, Y.-L. Yang, S.-B. Lei, C. Wang, On the topography multiplicity of non-planar titanyl (IV) phthalocyanine molecules and the STM imaging mechanism. *Surf. Sci.* **602**, 684–692 (2008).
59. W. S. Yun, S. W. Han, S. C. Hong, I. G. Kim, J. D. Lee, Thickness and strain effects on electronic structures of transition metal dichalcogenides: 2H-MX₂ semiconductors (*M* = Mo, W; *X* = S, Se, Te). *Phys. Rev. B* **85**, 033305 (2012).
60. W. Zhao, R. M. Ribeiro, M. Toh, A. Carvalho, C. Kloc, A. H. C. Neto, G. Eda, Origin of indirect optical transitions in few-layer MoS₂, WS₂, and WSe₂. *Nano Lett.* **13**, 5627–5634 (2013).

Acknowledgments

Funding: This work is supported by NSF grant DMR 1207213 and by LEAST (Low Energy Systems Technology)–STARnet, a Semiconductor Research Corporation (SRC) program, sponsored by the Microelectronics Advanced Research Corporation (MARCO), the Defense Advanced Research Projects Agency (DARPA), and by SRC NRI (Nanoelectronics Research Initiative) SWAN (South West Academy of Nanoelectronics). Y.G. would like to acknowledge the support from HPC Wales under project HPCW0285 for computational recourse. **Author contributions:** J.H.P. and A.C.K. conceived and designed this experiment. J.H.P. performed the STM experiments. J.H.P. and A.C.K. analyzed the STM/STS data. Y.G. performed the DFT calculations, and J.R. reviewed the calculations. Device fabrication and Raman were performed by A.S. and H.C.P.M. under the supervision of S.K.B. PL was performed by M.A. under the supervision of A.J. Growth of MoS₂ and SEM were performed by K.Z. under the supervision of J.A.R. All the data were discussed by J.H.P. and A.C.K. J.H.P. wrote most of the manuscript. The manuscript was written through contributions of all the authors. **Competing interests:** The authors declare that they have no competing interests. **Data and materials availability:** All data needed to evaluate the conclusions in the paper are present in the paper and/or the Supplementary Materials. Additional data related to this paper may be requested from the authors.

Submitted 18 May 2017

Accepted 20 September 2017

Published 20 October 2017

10.1126/sciadv.1701661

Citation: J. H. Park, A. Sanne, Y. Guo, M. Amani, K. Zhang, H. C. P. Movva, J. A. Robinson, A. Javey, J. Robertson, S. K. Banerjee, A. C. Kummel, Defect passivation of transition metal dichalcogenides via a charge transfer van der Waals interface. *Sci. Adv.* **3**, e1701661 (2017).